Regional Ventilation Changes in Severe Asthma after Bronchial Thermoplasty with ^{3}He MR Imaging and CT[1]

Robert P. Thomen, MS
Ajay Sheshadri, MD
James D. Quirk, PhD
Jim Kozlowski, BS
Henry D. Ellison
Rhonda D. Szczesniak, PhD
Mario Castro, MD, MPH
Jason C. Woods, PhD

Purpose: To quantify regional lung ventilation in healthy volunteers and patients with severe asthma (both before and after thermoplasty) by using a combination of helium 3 (^{3}He) magnetic resonance (MR) imaging and computed tomography (CT), with the intention of developing more effective image-guided treatments for obstructive lung diseases.

Materials and Methods: With approval of the local institutional review board, informed consent, and an Investigational New Drug Exemption, six healthy volunteers and 10 patients with severe asthma were imaged in compliance with HIPAA regulations by using both multidetector CT and ^{3}He MR imaging. Individual bronchopulmonary segments were labeled voxel by voxel from the CT images and then registered to the ^{3}He MR images by using custom software. The ^{3}He signal intensity was then analyzed by evaluating the volume-weighted fraction of total-lung signal intensity present in each segment (segmental ventilation percentage [SVP]) and by identifying the whole-lung defect percentage and the segmental defect percentage. Of the 10 patients with asthma, seven received treatment with bronchial thermoplasty and were imaged with ^{3}He MR a second time. Changes in segmental defect percentages and whole-lung defect percentages are presented.

Results: Ventilation measures for healthy volunteers yielded smaller segment-to-segment variation (mean SVP, 100% ± 18 [standard deviation]) than did the measures for patients with severe asthma (mean SVP, 97% ± 23). Patients with asthma also demonstrated larger segmental defect percentages (median, 13.5%; interquartile range, 8.9%–17.8%) than healthy volunteers (median, 6%; interquartile range, 5.6%–6.3%). These quantitative results confirm what is visually observed on the ^{3}He images. A Spearman correlation of $r = -0.82$ was found between the change in whole-lung defect percentage and the number of days between final treatment and second ^{3}He imaging.

Conclusion: Regional quantification of lung ventilation is indeed feasible and may be a useful technique for image-guided treatment of obstructive lung diseases, such as bronchial thermoplasty for severe asthma. In these patients, ventilation defects decreased as a function of time after treatment.

Online supplemental material is available for this article.

[1] From the Department of Physics, Washington University in St Louis, St Louis, Mo (R.P.T., H.D.E., J.C.W.); Department of Internal Medicine (A.S., J.K., M.C.) and Mallinckrodt Institute of Radiology (J.D.Q.), Washington University School of Medicine, St Louis, Mo; and Center for Pulmonary Imaging Research (R.P.T., J.C.W.) and Division of Biostatistics and Epidemiology (R.D.S.), Cincinnati Children's Hospital Medical Center, 3333 Burnet Ave, Cincinnati, OH 45229. Received January 13, 2014; revision requested March 19; final revision received May 9; accepted May 29; final version accepted June 18. **Address correspondence to** J.C.W. (e-mail: *jason.woods@cchmc.org*).

Hyperpolarized gas (helium 3 [^{3}He] and xenon 129 [^{129}Xe]) magnetic resonance (MR) imaging is quickly becoming a newly accepted research standard for investigation of regional lung function and microstructure (1–6) with high-spatial-resolution ventilation images and maps of alveolar geometry (5,7). To date, a clear quantification of regional ventilation and regional structure-function relationships and how they relate to potential therapeutic interventions has been lacking, partly because of an inability to segment ventilation images into anatomically correct bronchopulmonary segments (8). Advances in computed tomography (CT) analysis software (9) allow semiautomatic bronchopulmonary segmentation to be performed with detailed labeling out to subsegmental airway branches. In this study, we hypothesize that quantification of regional lung ventilation at the level of bronchopulmonary segments by using ^{3}He MR imaging and CT is feasible and that these methods can be used to measure regional changes in ventilation after bronchial thermoplasty. Our long-term motivation is to develop and implement imaging techniques to improve existing and emerging regional treatments for lung disease. For example, bronchoscopic treatment for chronic obstructive pulmonary disease with one-way valves (10–12) and/or lung volume reduction surgery (13) has the potential for regional trapped-gas removal and may be made more effective by using image guidance. Also, bronchoscopic lavage for pulmonary alveolar proteinosis currently occurs for the whole lung (14,15) and may benefit from this quantitative regional ventilation information.

Bronchial thermoplasty, the particular focus of this study, was approved by the U.S. Food and Drug Administration in 2010 for treatment of severe asthma (16), but reasons for its approval are largely clinical, not physiologic (17–21). The procedure involves bronchoscopy of the sedated patient and application of radiofrequency (RF) heating to the inner wall of branching airways via a small probe. Ablation of smooth muscle tissue in this manner reduces exacerbations and increases quality of life in a clinically and statistically significant way (21). The imaging methods presented here may pave the way toward image-guided regional treatment, which could potentially reduce the number of treatment sessions and obviate the ablation of less obstructed segments (22).

The goal of this article is twofold: first, to demonstrate that regional quantification of ventilation in individual bronchopulmonary segments is indeed feasible with a combination of ^{3}He MR imaging and CT and, second, to present preliminary results of observing segmental ventilation changes in patients with severe asthma before and after treatment by using bronchial thermoplasty. Currently, ventilatory function cannot easily be extracted from CT alone (23,24); likewise, MR imaging cannot provide adequate structural information for segmental delineation (25–27). With the use of the anatomic information available from CT, we were able to quantify regional ^{3}He ventilation in healthy volunteers and patients with severe asthma (some of whom were treated by using bronchial thermoplasty and underwent imaging with ^{3}He a second time). As expected (28,29), individual anatomic variation among patients or volunteers is sizeable; individual lung segment maps are therefore necessary for accurate assessment. Ventilation defects increased for early posttreatment times and decreased for late treatment times. In this work, we aimed to quantify regional lung ventilation in healthy volunteers and patients with severe asthma (both before and after thermoplasty) at the level of individual bronchopulmonary segments by using a combination of ^{3}He MR imaging and CT, with the intention of developing more effective image-guided treatments for obstructive lung diseases.

Advances in Knowledge

- A method of quantification of segmental lung ventilation in individual bronchopulmonary segments in patients with severe asthma is demonstrated, on the basis of individual anatomic data; the median whole-lung defect percentage was 6.0% (interquartile range, 5.6%–6.3%) in healthy volunteers and 13.5% (interquartile range, 8.9%–17.8%) in patients with severe asthma ($P < .005$).
- Ventilation defects decrease as a function of time after bronchial thermoplasty ($r = -0.82$, $n = 7$, $P < .04$).

Implication for Patient Care

- Hyperpolarized gas MR imaging may be used to quantify segmental ventilation defects before and after therapies.

Materials and Methods

Imaging Methods

With approval of our local institutional review board (Washington University in St Louis, St Louis, Mo), informed consent, and an Investigational New Drug Exemption, six healthy volunteers (no history of pulmonary disease or abnormality) and 10 patients with severe

Published online before print
10.1148/radiol.14140080 **Content codes:** CH CT MR

Radiology 2015; 274:250–259

Abbreviations:
FEV_1 = forced expiratory volume in the 1st second of expiration
LB = left lung segment
RB = right lung segment
RF = radiofrequency
SVP = segmental ventilation percentage

Author contributions:
Guarantors of integrity of entire study, R.P.T., J.C.W.; study concepts/study design or data acquisition or data analysis/interpretation, all authors; manuscript drafting or manuscript revision for important intellectual content, all authors; approval of final version of submitted manuscript, all authors; literature research, R.P.T., R.D.S., M.C., J.C.W.; clinical studies, A.S., J.D.Q., M.C., J.C.W.; experimental studies, R.P.T., J.D.Q., J.C.W.; statistical analysis, R.P.T., H.D.E., R.D.S., J.C.W.; and manuscript editing, R.P.T., A.S., J.D.Q., H.D.E., R.D.S., M.C., J.C.W.

Funding:
This research was supported by the Severe Asthma Research Program, National Institutes of Health (grant U10 HL109257).

Conflicts of interest are listed at the end of this article.

Table 1

Baseline Demographics

Variable	Healthy Volunteers ($n = 6$)	Patients with Severe Asthma ($n = 10$)	*P* Value*
Age at date of entry (y)†	22.5 (22–24.5)	42.5 (40.25–45.75)	<.001
Sex‡			
Male	33 (2)	40 (4)	>.6
Female	67 (4)	60 (6)	>.99
Age (y)§			
Male	20.5 (19–22)	41 (37–45)	< .002
Female	23.3 (22–25)	43.7 (31–51)	< .001
White‡	67 (4)	60 (6)	>.99
Body mass index (kg/m^2)†	25.8 (22–29.1)	34.1 (30.5–36.2)	.011
Age at onset (y)†	NA	10 (2–29)	NA
Duration of asthma (y)§	NA	27.7 ± 17.3	NA
Immunoglobulin E (IU/mL)†	26.3 (16–80)	187 (137–240)‖	.022
Percentage of peripheral blood eosinophils in blood†	1.25 (1.03–1.78)	1.75 (1–2)	.587
Percentage of blood eosinophils in sputum†	0 (0–0.4)#	0.9 (0.1–7.1)	.164
Atopy, with positive allergy skin test‡	83 (5)	90 (9)	>.99
FEV_1 after bronchodilator use (L)†	3.59 (3.1–4.4)	2.44 (2.3–2.6)	.03
After therapy ($n = 6$)**	NA	2.18 (1.8–2.4)	NA
FEV_1, percentage predicted†	108 (91–113)	78 (69–83)	.002
After therapy ($n = 6$)**	NA	69 (62–73)	NA
Asthma Quality of Life Questionnaire median score††	NA	3.94 (3.50–4.34)	NA
After therapy ($n = 7$)††	NA	4.88 (3.75–6.00)	NA

Note.—FEV_1 = forced expiratory volume in the 1st second of expiration, NA = not applicable.

* The Mann-Whitney-Wilcoxon test was used for *P* values for continuous variables, and the Fisher exact test was used for the *P* values for categorical variables.

† Data are medians, and numbers in parentheses are interquartile ranges.

‡ Data are percentages, and numbers in parentheses are numbers of subjects.

§ The Student *t* test gives no significant difference between male and female participants in either the population of healthy volunteers or the population of patients with severe asthma. Data are means, with age ranges in parentheses.

‖ Immunoglobulin E level was reported in seven of 10 patients with asthma.

Percentage of peripheral blood eosinophils in sputum was reported in five of six healthy volunteers.

** Second FEV_1 after bronchodilator use after thermoplasty was not reported for patient 6 with asthma; posttreatment FEV_1 values were acquired 6 weeks following final therapy session.

†† A change of more than 0.5 in the Asthma Quality of Life Questionnaire score is considered clinically significant; all scores were acquired within 2 years following final treatment.

asthma (patient data given in Table 1) underwent CT and MR imaging in compliance with Health Insurance Portability and Accountability Act regulations. CT (Definition; Siemens, Munich, Germany) was performed with the following: 0.5–0.7-mm sections, 80–145 mAs based on body mass index, 0.4–0.7-mm in-plane resolution, and a 512 × 512 matrix, with images acquired at total lung capacity. ^{3}He MR imaging (Avanto; Siemens) at 1.5 T was performed with a two-dimensional gradient-echo sequence and the following: repetition time msec/echo time msec, 140/3; 10–15-mm sections; 3–4-mm in-plane resolution; and a 64 × 128 matrix, with images acquired at functional residual capacity plus 1 L. All subjects were maximally bronchodilated (following our standard protocol [29]) before imaging in an attempt to eliminate reversible airway obstruction from the images. Of the 10 patients with asthma who were imaged, seven underwent treatment with bronchial thermoplasty and subsequently underwent imaging with ^{3}He MR imaging a second time for comparison of findings with the findings in the healthy volunteer group, which behaves as our control group. Hyperpolarized ^{3}He gas was prepared by using either a homebuilt or commercial (IGI.9600.3He; GE Healthcare, Durham, NC) ^{3}He polarizer implementing spin-exchange optical pumping to approximately 30% polarization (30). Subjects were coached to exhale to functional residual capacity and then to inhale a 1-L ^{3}He gas mixture of approximately 30% ^{3}He and 70% N_2. The ^{3}He images were acquired by using a volume-transmit and eight-channel phased-array receiver coil during a 9-second breath hold.

Image Analysis

CT images were analyzed with software (Apollo; Vida Diagnostics, Coralville, Iowa), which allows for semiautomatic segmentation and labeling of individual bronchopulmonary segments by examining the airway and vascular branching. All masks were verified by an expert in pulmonary anatomy (A.S. or J.K., with more than 2 years of experience each). The software returns a collection of "mask" images where individual pixels are assigned integer values

corresponding to each of the bronchopulmonary segments. Because the ^{3}He MR imaging and CT are performed during different sessions and at slightly different lung volumes, the mask images had to be registered to the ^{3}He lung images for analysis. The CT images must be acquired at total lung capacity, as this yields more accurate airway segmentation. Custom software (Matlab; MathWorks, Natick, Mass) employing a user-guided landmark-based approach has been developed for this purpose. A user-guided registration method was chosen over more automatic, gradient-based approaches because ^{3}He MR images in patients with lung disease often contain regions of defective ventilation, which would yield incorrect registration.

Registration Process

The registration algorithm is a two-step process that involves, first, matching an appropriate CT section to each ^{3}He section by assessing anatomic features (eg, blood vessels and airways) and, then, selecting corresponding anatomic points within the matched sections for the registration landmarks. The process of assigning a CT section (0.5–0.7-mm thickness) to each ^{3}He section (10–15 mm) involves individually examining each ^{3}He image, determining section location relative to the carina, and locating the stack of CT images corresponding to that geographic CT level. Within that 10–15-mm stack, the best CT match was chosen by assessing the various anatomic features, such as blood vessels, airways, or apparent partial volumes (eg, diaphragm). The user separately registers each lung in the CT image to its ^{3}He counterpart by selecting points around the CT and ^{3}He lung contour to be matched. Using two-dimensional surface fitting based on Delaunay triangulation, selected coordinates of the CT image are mapped to those of the ^{3}He image, and the corresponding CT mask is registered by using cubic interpolation. The mask is then downsized to fit the resolution of the ^{3}He image by using nearest-neighbor interpolation. Representative images illustrating this process are given in Figure 1.

Figure 1

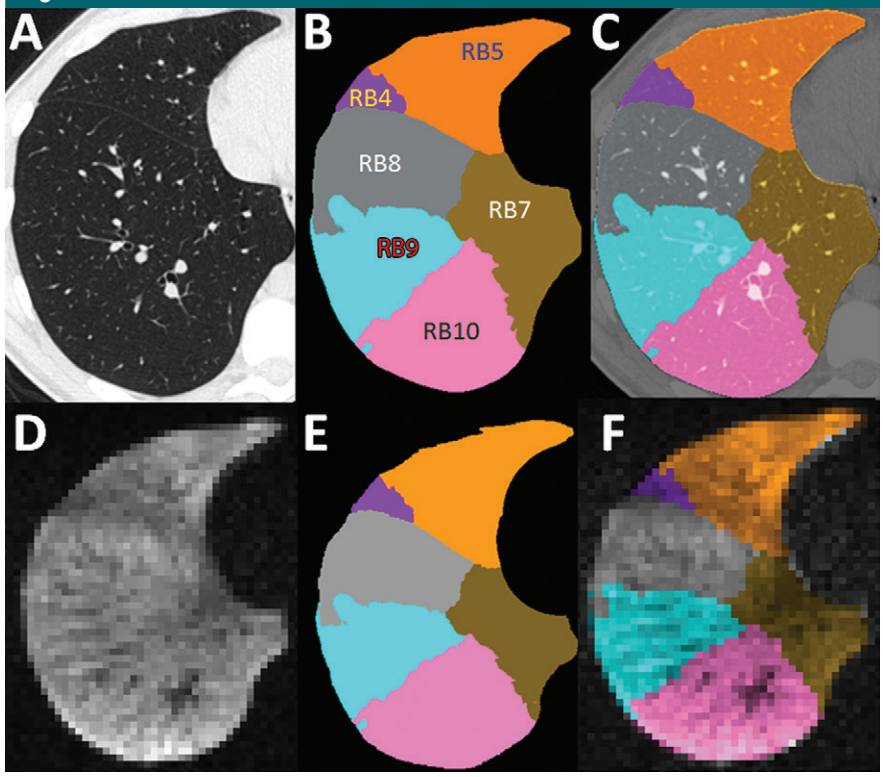

Figure 1: Illustration of the registration process. *A,* Raw axial CT image of a lower-medial right lung section in a healthy volunteer. *B,* CT section mask image with bronchopulmonary segments labeled. *C,* CT image with mask image superimposed. *D,* ^{3}He MR image (140/3) corresponding to the CT section. *E,* Mask image of *B* registered to match the ^{3}He lung contour in *D*. *F,* Registered mask superimposed on the ^{3}He section illustrating segmental separation. CT dose varied according to body mass index: less than 20 kg/m^2, 80 mAs; 20–30 kg/m^2, 100 mAs; more than 30 kg/m^2, 145 mAs. RB = right lung segment.

RF Correction

Because ^{3}He MR imaging was performed with a flexible eight-channel coil receiver array (half across the subject's back, with the other half across the chest), the raw ^{3}He images demonstrate RF sensitivity profiles that change slightly from anterior to posterior and from apex to base. This RF sensitivity variation is smooth and consistent and was quantified in both of these directions according to the sensitivity profile exhibited in the healthy volunteers by fitting a third-order polynomial to the healthy averages. This allowed for an effective flattening of the RF-sensitivity profiles for quantification to simplify the segmental analysis described below. The expected gravitational dependence in the anterior-to-posterior profile (31,32) was not suppressed; anterior-to-posterior sensitivity is symmetric and was characterized according to the anterior coil and mirrored to provide the posterior normalization, thus preserving necessary gravitational ventilation information.

Segmental Analysis

With the use of the registered masks and ^{3}He images, each segment's fraction of total ^{3}He signal intensity is measured and compared with the fractional total lung volume of each segment measured in voxels by using the registered CT masks. The signal fraction divided by the volume fraction yields a number characteristic of average ventilation of the entire segment, named the *segmental ventilation percentage* (SVP). For instance, if a particular segment, the left lung segment (LB) 9, contains 4% of the total ^{3}He lung signal intensity and

makes up 5% of the total lung volume, then LB9 is assigned an SVP of 80%, which is calculated as 0.04/0.05. For patients with regional obstructive lung diseases, there will be segments whose SVPs are below and above 100%. It is important to note that, although this is a useful method of quantifying ventilation of an entire segment, it is possible for defective regions of the lung to be subsegmental; thus, an individual segment could contain regions of both low and high ventilation, thereby obscuring apparent ventilation abnormalities if one uses SVPs alone for quantitation.

Defect Analysis

Evaluating the fraction of lung volume containing ventilation defects is an established method of evaluating overall lung ventilation (33–37). Lung defect calculations—total and segmental defect percentages—were performed by evaluating the percentage of voxels whose signal intensity was below a threshold of 60% of the total lung mean signal intensity. This value (60%) represents our estimate of the visually accurate defect selection threshold for all patients with asthma and was automated into the ventilation analysis. Figure 2 shows a plot of total-lung defect percentage as a function of threshold, validating this choice as maximizing contrast between groups. This approach also necessitates the RF profile correction described earlier. We next applied a median filter (3 × 3 kernel) to each section of the calculated defect array to remove defect artifacts, which often occur at blood vessels, and single-voxel partial volumes at the lung peripheries. These are the primary sources of initially apparent defects in data for the healthy volunteers, and the median filter appropriately reduces the number of inaccurately labeled defect voxels, thus providing more reliable contrast between data for healthy volunteers and data for patients with asthma. While other authors have developed more elaborate approaches to defect identification (2,33), this method is simple and serves our purpose of effectively emulating the process of manual defect selection by a radiologist while maintaining quantitative objectivity. It thus relates more directly to potential treatment algorithms for bronchial thermoplasty.

Figure 2

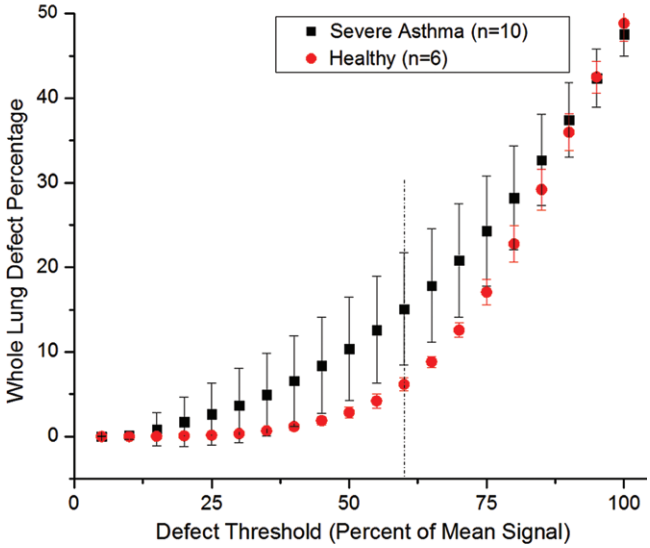

Figure 2: Plot of the calculated whole-lung defect percentage as a function of the defect threshold for averaged data sets in healthy volunteers and patients with asthma. Dashed line = the chosen threshold of 60% (maximizing the contrast between healthy volunteers and patients with asthma). Error bars = standard deviations among subjects (healthy volunteers, $n = 6$; patients with asthma, $n = 10$).

Bronchial Thermoplasty Assessment

Of the 10 patients with severe asthma who underwent imaging, seven were treated with bronchial thermoplasty and underwent ^{3}He MR imaging a second time from 40 to 104 days after the final treatment, on the basis largely of the imaging unit and patient availability. It has been shown in several studies that patients who undergo bronchial thermoplasty often experience more exacerbations and require more hospitalizations in the first 90 days following treatment (21), and we have chosen to characterize patients according to the number of days between final treatment and second ^{3}He imaging.

Statistical Methods

Descriptive analyses were performed by two authors (R.T. and R.S.), with calculation of means, standard deviations, and quartiles for continuous data and proportions for nominal data. Correlation between two variables was assessed by using the Spearman correlation coefficient. Subject characteristics of healthy volunteers and patients with severe asthma were compared by using the Mann-Whitney-Wilcoxon test for continuous variables and the Fisher exact test for nominal variables (Table 1). Descriptive statistics for SVP results are expressed as means ± standard deviations, and defect percentages are expressed as medians and interquartile ranges, unless stated otherwise.

Two distinct types of repeated measures arise from the SVP data collection. First, there are multiple segments measured for each subject; second, in some of the patients with asthma, measurements are made at two distinct points in time (before and after bronchial thermoplasty). Linear mixed-effects models for nested repeated measures (38) are used to examine differences in SVP between patients with asthma and healthy volunteers, as well as within patients with asthma in whom measurements were made both before and after bronchial thermoplasty. This

Figure 3

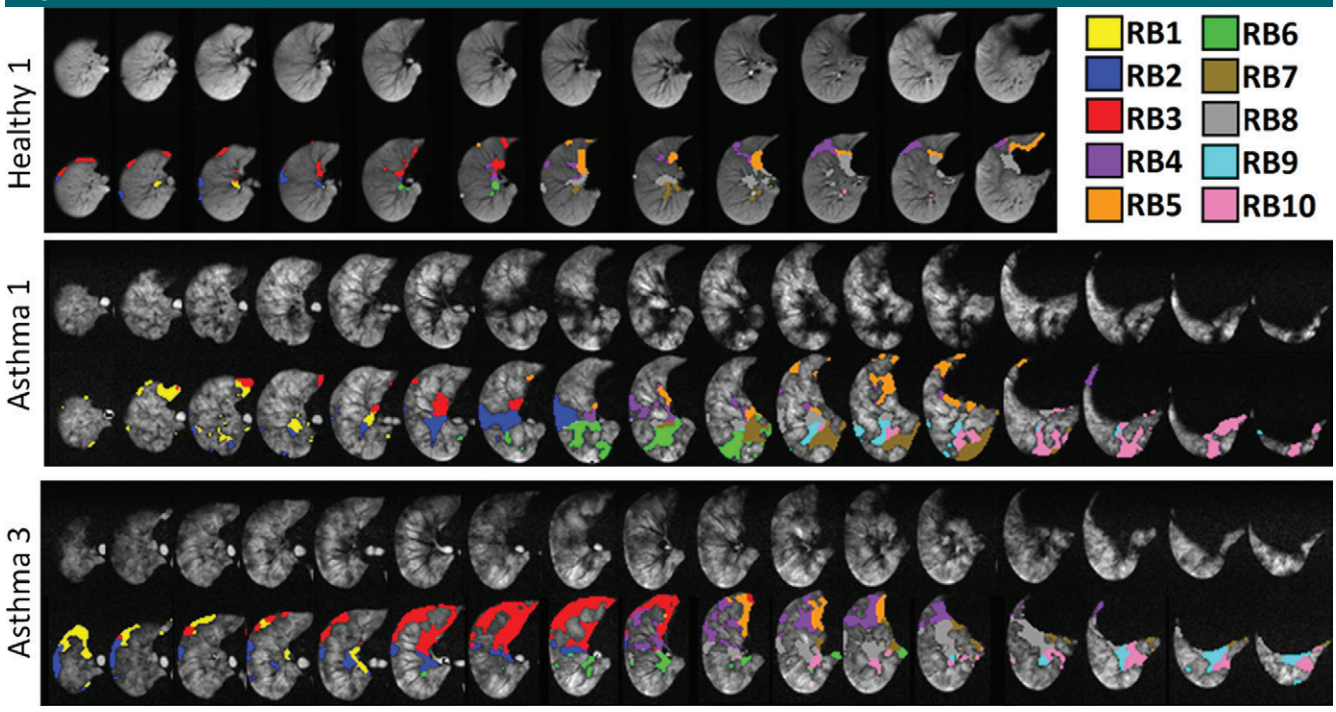

Figure 3: Sets of images illustrating defects for the right lungs of healthy volunteer 1 and patients 1 and 3 with severe asthma. Defect voxels are colored according to their respective bronchopulmonary segments in the second row at top, middle, and bottom. CT dose varied according to body mass index: less than 20 kg/m^2, 80 mAs; 20–30 kg/m^2, 100 mAs; more than 30 kg/m^2, 145 mAs. MR parameters were 140/3. Numeric data are given in Tables E1 and E2 (online), and a bar plot of segmental data is shown in Figure 4.

approach is used to examine the association between SVP and defect percentages, overall and with respect to the aforementioned group comparisons, by including defect percentage as a covariate in the model and its corresponding interactions with group. Differences in subjects with asthma before and after bronchial thermoplasty are examined by using a separate model, because only a subset of patients with asthma have data available at both times. In each model, random effects are used to account for the repeated-measures factors. To meet normality assumptions, SVP was log transformed for model analyses. Model results have been back-transformed to the original scale and are presented with 95% confidence intervals.

Results

Exploratory analysis showed that the six healthy volunteers, on average, had similar ventilation across segments (mean, 100% ± 18 [standard deviation] for all SVPs; range, 63%–136%; 114 segments), with the consistent exceptions of RB4 (mean, 78% ± 8) and RB5 (mean, 76% ± 12). By contrast, the 10 patients with asthma had SVPs that averaged 97% ± 23 and ranged from 34% to 172% (190 segments). As expected, the average of all SVPs in healthy volunteers and patients with severe asthma is near 100%, while the standard deviation for patients with asthma is larger; Table E1 (online) details complete SVP data. The mixed-model results suggest a similar mean SVP for each group. The mean SVP for healthy volunteers is 99.5% (95% confidence interval: 95.4, 103.6); the asthma patient group has a slightly lower mean SVP of 97.4% (95% confidence interval: 96.2, 102.8), but the difference is not significant. Patients with asthma do not experience a significant difference in SVP after bronchial thermoplasty, but the mean SVP of 96.7% is slightly lower (95% confidence interval: 92.2, 101.2). Representative ^{3}He images illustrating masking and defect identification are shown in Figure 3 for right lungs in a healthy volunteer and asthma patients 1 and 3 (chosen to illustrate contrasting regional defects). The median whole-lung defect percentage of the healthy volunteers was 6.0% (interquartile range, 5.6%–6.3%), and that for patients with asthma was 13.5% (interquartile range, 8.9%–17.8%) ($P < .005$). As expected, whole-lung defect percentages in patients with severe asthma increase more quickly as a function of defect threshold than in healthy volunteers. The greatest difference in defect percentage between healthy volunteer population and the population of patients with asthma was approximately 55%–65% of the mean, justifying our choice of 60% for the defect threshold. All SVPs and segmental defect percentages are given in Tables E1 and E2 (online). Larger segmental

Figure 4

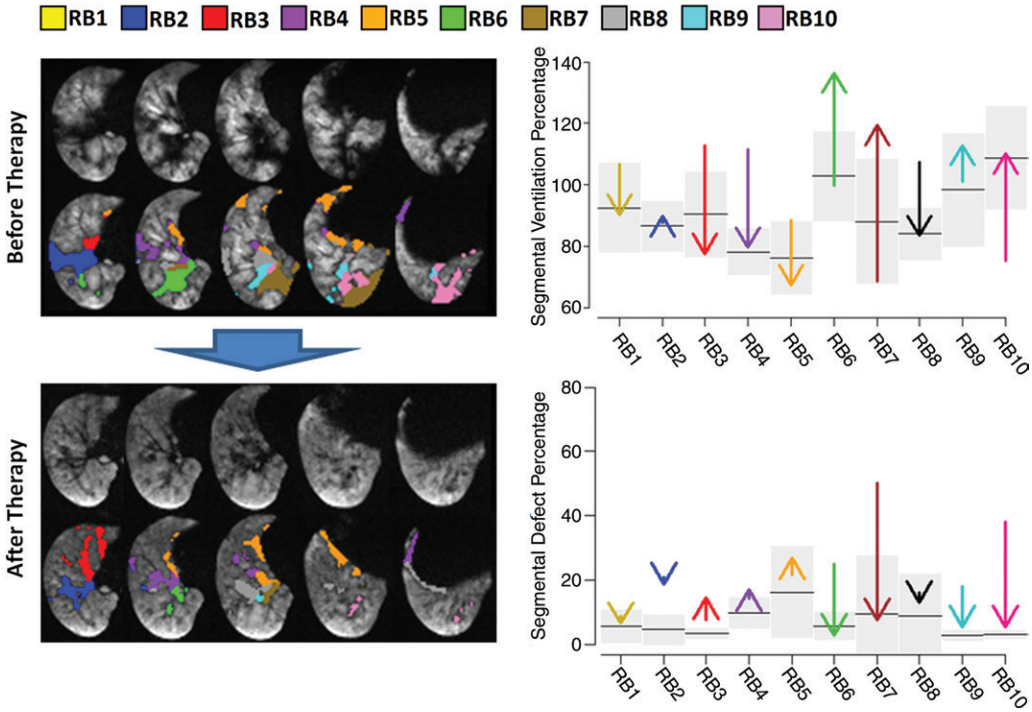

Figure 4: Example of ventilation changes in response to bronchial thermoplasty for patient 1 with asthma (91 days between final therapy and imaging). Selected ^{3}He sections are shown (with and without defect voxels labeled according to segment), along with arrow plots showing right-lung segmental defect percentages and SVP before and after bronchial thermoplasty (arrowhead indicates posttreatment value). For segmental ventilation percentages, the black line in each segment is the mean; for defect percentages, the black line is the median. Gray boxes span 1 standard deviation for segmental ventilation percentages and span the interquartile range for defect percentages ($n = 6$). Numeric data are given in Tables E1 and E2 (online). CT dose varied according to body mass index: less than 20 kg/m^2, 80 mAs; 20–30 kg/m^2, 100 mAs; more than 30 kg/m^2, 145 mAs. MR parameters were 140/3. Large blue arrow indicates progression of time; images before therapy proceed to become second set of images after treatment.

defect percentages strongly associate with smaller SVPs (linear mixed model coefficient $r = -1.6$ [95% confidence interval: -1.9, -1.3]; $P < .0001$). Furthermore, this negative association is stronger in healthy volunteers, compared with patients with asthma (difference between coefficients: -0.4 [95% confidence interval: 0.1, 0.7]; $P = .0174$). The relationship between SVPs and segmental defect percentages was similar before and after bronchial thermoplasty (before vs after: -0.1 [95% confidence interval: -0.2, -0.1]).

In patients who underwent bronchial thermoplasty (seven of the 10 patients with asthma), a Spearman correlation of -0.82 was found between the number of days between final treatment and change in whole-lung defect percentage ($n = 7$, $P < .04$). Numeric data are given in Table E2 (online). Figure 4 shows representative sections from asthma patient 1, with labeled defect voxels and plots illustrating the corresponding changes in defect and ventilation percentages before and after treatment.

Discussion

Here, we have presented a method for characterizing individual bronchopulmonary segments according to their SVPs and their within-segment defect percentages. We have applied these methods in healthy volunteers and patients with severe asthma both before and after treatment with bronchial thermoplasty. Comparing the SVPs with the findings on ^{3}He images confirms that the SVPs are consistent with a visual assessment of regional ventilation and defects (Fig 3; Tables E1, E2 [online]), as expected. Uniform ventilation across segments, characteristic of the healthy volunteer population, was indeed revealed by the lower standard deviation across SVPs in healthy volunteers. There were age and body mass index differences between the control group and the severe asthma group; both likely result in our control group having fewer ventilation defects than in a well age-matched group (39). Nevertheless even older healthy volunteers generally have uniform ventilation compared with patients with severe asthma, and we expect that the age differences between control and

Table 2

Individual Patient Data

Patient No.	Age (y)	Sex	BMI (kg/m^2)	FEV_1 before BT*		Predicted FEV_1 (L)	FEV_1 after BT†	
				Before Bronchodilation	After Bronchodilation		Before Bronchodilation	After Bronchodilation
Patients with severe asthma								
With BT								
1	42	M	36.2	1.94/60	2.17/67	3.23	1.77/55	2.15/67
2	45	M	27.9	2.45/74	2.68/81	3.32	2.47/74	2.46/74
3	50	F	41.4	1.28/60	1.40/66	2.13	1.22/57	1.49/70
4	46	F	38.8	2.25/78	2.41/83	2.9	1.86/64	1.73/60
5	40	M	32.2	2.7/64	2.87/68	4.2	1.94/46	2.20/52
6	51	F	29.9	2.35/92	2.46/96	2.56	. . .	. . .
7	43	F	24.6	2.37/73	2.52/78	3.24	2.43/75	2.62/81
Without BT								
8	37	M	34.7	2.09/61	2.62/77	3.42	. . .	. . .
9	41	F	33.4	1.83/56	2.33/72	3.24	. . .	. . .
10	31	F	36.1	2.15/87	2.38/97	2.46	. . .	. . .
Healthy volunteers								
1	25	F	27.2	2.36/86	2.39/87	2.74	. . .	. . .
2	22	M	19.4	4.41/106	4.65/112	4.15	. . .	. . .
3	23	F	33	3.56/99	3.7/103	3.58	. . .	. . .
4	22	F	24.3	2.97/84	2.98/84	3.54	. . .	. . .
5	25	F	29.7	3.41/114	3.47/116	2.98	. . .	. . .
6	19	M	21.2	5.12/103	5.64/113	4.98	. . .	. . .

Note.—BMI = body mass index, BT = bronchial thermoplasty.

* Spirometry was performed at the time of CT. FEV_1 values are in liters/percentage predicted.

† Spirometry was performed 6 weeks following the final therapy session. FEV_1 values are in liters/percentage predicted.

asthma groups (Tables 1, 2) contribute negligibly to any differences (3,40–42).

Because the presence of ventilation defects is determined by the mean signal intensity value across the whole lung, heterogeneous signal within individual segments may not yield low SVPs but can still contain large defect percentages. Conversely, because the SVP is inherently weighted by individual segment volumes, uniformly low ventilation within a large segment may not necessarily contain many defect voxels but will still yield informative (low) SVPs. For example, segment RB8 in patient 1 was hyperventilated (high SVP) before therapy, and this measure decreased after therapy; the segmental defect percentage also decreased, reflecting an increased homogeneity within that segment, consistent with increased homogeneity between segments throughout the lung. We believe these two segmental measures complement each other well, since SVPs help reveal intersegment abnormalities, while the segmental defect calculation reveals within-segment abnormalities. Stark intersegmental abnormalities are of course revealed by both measures. Further, these segmental- and whole-lung defect percentages and intersegmental SVP variation can reveal whole-lung ventilation information where desired.

The strong negative association between SVPs and defect percentages implies, as expected, that segments with low ventilation tend to have high defect percentages (patient 4, segments RB8, RB9, RB10 in Tables E1 and E2 [online]), but indeed this is not always the case and the information is not redundant (patient 4, LB6; and patient 8, LB3). Results indicate that ventilation in the right middle lobe (RB4 and RB5) is consistently low across all subjects, including healthy volunteers (as evidenced in images in Fig 3). It is not clear from where this arises; we do not believe that it is a systematic error and have therefore made no corrections to the signal in response. However, this would imply that defect percentages should be higher in the right lung; Tables E1 and E2 (online) do indeed indicate this finding.

Mislabeled pixels due to error in segmentation and registration are a limitation of this method. The software (Apollo; Vida Diagnostics) requires user intervention in its segmentation for appropriate segment labeling, but it has been validated both technically and clinically (9,43). On average, about 5% of all pixels in a given registered image can potentially be mislabeled by registration error (established by evaluating the number of mismatched pixels in 10 registrations of the same mask). Each reported SVP and defect percentage has an estimated relative error of 4% and 5%, respectively, on the basis of this analysis, which is smaller than the biologic variation seen in healthy volunteers (Tables E1, E2 [online]). We

believe this presents little concern for our ultimate goal of image guidance in therapy, but we recognize it as a valid source of segmental quantification error. Further, bronchial thermoplasty currently focuses on lobar treatment, and this method quantifies ventilation to the third generation (segments). Because the 10–15-mm section thickness makes the ^{3}He sections much thicker than their CT counterparts, care is taken to examine all potential CT sections for appropriate anatomic matching.

Another limitation of this study is the lack of clinical tests that were administered at the same time as imaging (Tables E1, E2 [online]). Although pulmonary function tests were administered before and after therapy, posttherapy pulmonary function tests were performed 6 weeks following final therapy (as opposed to ^{3}He imaging, which was performed anywhere from 40–104 days following final treatment because of MR imaging scheduling). Asthma Quality of Life Questionnaires were also administered to each patient before and after treatment, but no posttreatment results were obtained fewer than 100 days following final treatment. Thus, correlations between pulmonary function test or quality-of-life changes and imaging changes would be misleading here. It should be noted, however, that the delayed recovery trend seen in previous studies following treatment is still apparent from both the clinical data and imaging data: FEV_1 collectively decreased at 6 weeks after treatment, quality-of-life scores increased at more than 14 weeks (Tables 1, 2), and ventilation defects increased and then decreased as a function of imaging time after treatment.

With the use of segmental ventilation quantification, regional structure-function relationships can be more effectively examined and quantified. For instance, subsegmental regions of hypoventilation may indicate decreased airway lumen in subsegmental airways, and near-zero ventilation may indicate complete airway collapse or a mucus plug. This regional analysis may also be useful in longitudinal studies to monitor airway improvement or response to various global or regional treatments (42). In the case of bronchial thermoplasty examined more closely here, our imaging results complement those of past nonimaging, clinical studies (18–21), but with the regional specificity inherent in imaging. Although the trend is subtle, the correlation between length of time after treatment and change in whole-lung defect percentage ($r = -0.82$) indicates that ventilation imaging may indeed be a sensitive biomarker of the physiologic and clinical responses demonstrated by patients. Changes in gas distribution within the lung at the segmental level may prove useful in clinical translation. While we used ^{3}He here, we see no major impediments to using ^{129}Xe similarly.

We demonstrated that quantification of regional pulmonary ventilation at the segmental level is indeed feasible and confirms what is observed visibly. These techniques may be used to study regional structure-function relationships and in longitudinal evaluation in clinical trials of various pulmonary interventions. We demonstrated the capability of our analysis to quantify regional ventilation changes in patients with severe asthma, both before and after treatment with bronchial thermoplasty, and found that the defects in ventilation are consistent with data in the previous clinical studies. In particular, ventilation defects increase for earlier posttreatment times but decrease for later posttreatment times. We envision that this finding can be used to guide bronchial thermoplasty in particular but may be useful for any treatment that benefits from regional information about disease severity. For example, having a quantitative measure indicating the relative ventilation of differing segments (such as the SVPs are meant to address) may allow a pulmonologist to make judicious decisions concerning RF dose, the time between treatment sessions, or whether all treatment sessions are even necessary.

Disclosures of Conflicts of Interest: R.P.T. disclosed no relevant relationships. **A.S.** disclosed no relevant relationships. **J.D.Q.** disclosed no relevant relationships. **J.K.** disclosed no relevant relationships. **H.D.E.** disclosed no relevant relationships. **R.D.S.** disclosed no relevant relationships. **M.C.** Financial activities related to the present article: institution received grant no. U10 HL109257 from the Severe Asthma Research Program, National Institutes of Health. Financial activities not related to the present article: author received payment for consulting from Asthmatx/Boston, IPS/Holaira, and Neostem and received payment for consulting and serving on Advisory Board from Genentech; institution received industry-sponsored grants or has grants pending from Boston Scientific, Amgen, Ception/Cephalon/Teva, Genentech, Medimmune, Merck, Novartis, GSK, Sanofi Aventis, Vectura, Next Bio, and KaloBios; author received payment for service as speaker from GSK, Genentech, Boston Scientific, Boehringer Ingelheim, and Teva; author received royalties from Elsevier; and author receives stock or stock options from Sparo Inc. Other relationships: none to disclose. **J.C.W.** disclosed no relevant relationships.

References

1. Möller HE, Chen XJ, Saam B, et al. MRI of the lungs using hyperpolarized noble gases. Magn Reson Med 2002;47(6):1029–1051.
2. Fain S, Schiebler ML, McCormack DG, Parraga G. Imaging of lung function using hyperpolarized helium-3 magnetic resonance imaging: review of current and emerging translational methods and applications. J Magn Reson Imaging 2010;32(6):1398–1408.
3. Castro M, Fain SB, Hoffman EA, et al. Lung imaging in asthmatic patients: the picture is clearer. J Allergy Clin Immunol 2011; 128(3):467–478.
4. Leawoods JC, Yablonskiy DA, Saam B, Gierada DS, Conradi MS. Hyperpolarized ^{3}He gas production and MR imaging of the lung. Concepts Magn Reson 2001;13(5):277–293.
5. Biederer J, Both M, Graessner J, et al. Lung morphology: fast MR imaging assessment with a volumetric interpolated breath-hold technique—initial experience with patients. Radiology 2003;226(1):242–249.
6. Kuethe DO, Adolphi NL, Fukushima E. Short data-acquisition times improve projection images of lung tissue. Magn Reson Med 2007; 57(6):1058–1064.
7. Quirk JD, Lutey BA, Gierada DS, et al. In vivo detection of acinar microstructural changes in early emphysema with (3)He lung morphometry. Radiology 2011;260(3):866–874.
8. Tustison NJ, Avants BB, Flors L, et al. Ventilation-based segmentation of the lungs using hyperpolarized (3)He MRI. J Magn Reson Imaging 2011;34(4):831–841.
9. Tschirren J, Hoffman EA, McLennan G, Sonka M. Intrathoracic airway trees: seg-

mentation and airway morphology analysis from low-dose CT scans. IEEE Trans Med Imaging 2005;24(12):1529–1539.

10. Galluccio G, Lucantoni G. Bronchoscopic lung volume reduction for pulmonary emphysema: preliminary experience with a new NOVATECH endobronchial silicone one-way valve. Interact Cardiovasc Thorac Surg 2010;11(2):213–215.
11. Lausberg HF, Chino K, Patterson GA, Meyers BF, Toeniskoetter PD, Cooper JD. Bronchial fenestration improves expiratory flow in emphysematous human lungs. Ann Thorac Surg 2003;75(2):393–397; discussion 398.
12. Sethi S, Cicenia J. TReatment of pcp-related pneumothorax using one-way endobronchial valves [abstr]. Chest J 2008;134(4_Meeting-Abstracts):9002.
13. Zahid I, Sharif S, Routledge T, Scarci M. Is lung volume reduction surgery effective in the treatment of advanced emphysema? Interact Cardiovasc Thorac Surg 2011;12(3):480–486.
14. Trapnell BC, Carey BC, Uchida K, Suzuki T. Pulmonary alveolar proteinosis, a primary immunodeficiency of impaired GM-CSF stimulation of macrophages. Curr Opin Immunol 2009;21(5):514–521.
15. Suzuki T, Sakagami T, Young LR, et al. Hereditary pulmonary alveolar proteinosis: pathogenesis, presentation, diagnosis, and therapy. Am J Respir Crit Care Med 2010;182(10):1292–1304.
16. U.S. Food and Drug Administration. Approval of Alair Bronchial Thermoplasty System: Alait Catheter and Alair RF Controller. Silver Spring, Md: U.S. Food and Drug Administration, 2010.
17. Miller JD, Cox G, Vincic L, Lombard CM, Loomas BE, Danek CJ. A prospective feasibility study of bronchial thermoplasty in the human airway. Chest 2005;127(6):1999–2006.
18. Cox G, Thomson NC, Rubin AS, et al. Asthma control during the year after bronchial thermoplasty. N Engl J Med 2007;356(13):1327–1337.
19. Pavord ID, Cox G, Thomson NC, et al. Safety and efficacy of bronchial thermoplasty in symptomatic, severe asthma. Am J Respir Crit Care Med 2007;176(12):1185–1191.
20. Castro M, Rubin AS, Laviolette M, et al. Effectiveness and safety of bronchial thermoplasty in the treatment of severe asthma: a multicenter, randomized, double-blind, sham-controlled clinical trial. Am J Respir Crit Care Med 2010;181(2):116–124.
21. Gildea TR, Khatri SB, Castro M. Bronchial thermoplasty: a new treatment for severe refractory asthma. Cleve Clin J Med 2011;78(7):477–485.
22. Cox G, Miller JD, McWilliams A, Fitzgerald JM, Lam S. Bronchial thermoplasty for asthma. Am J Respir Crit Care Med 2006;173(9):965–969.
23. Khadadah M, Jayakrishnan B, Muquim A, et al. High resolution computed tomography in asthma. Oman Med J 2012;27(2):145–150.
24. Aliverti A, Pennati F, Salito C, Woods JC. Regional lung function and heterogeneity of specific gas volume in healthy and emphysematous subjects. Eur Respir J 2013;41(5):1179–1188.
25. Fain SB, Gonzalez-Fernandez G, Peterson ET, et al. Evaluation of structure-function relationships in asthma using multidetector CT and hyperpolarized He-3 MRI. Acad Radiol 2008;15(6):753–762.
26. Ireland RH, Woodhouse N, Hoggard N, et al. An image acquisition and registration strategy for the fusion of hyperpolarized helium-3 MRI and x-ray CT images of the lung. Phys Med Biol 2008;53(21):6055–6063.
27. Woodhouse N, Wild JM, Paley MN, et al. Combined helium-3/proton magnetic resonance imaging measurement of ventilated lung volumes in smokers compared to never-smokers. J Magn Reson Imaging 2005;21(4):365–369.
28. Altes TA, Powers PL, Knight-Scott J, et al. Hyperpolarized 3He MR lung ventilation imaging in asthmatics: preliminary findings. J Magn Reson Imaging 2001;13(3):378–384.
29. Busacker A, Newell JD Jr, Keefe T, et al. A multivariate analysis of risk factors for the air-trapping asthmatic phenotype as measured by quantitative CT analysis. Chest 2009;135(1):48–56.
30. Happer W. Spin exhange, past, present, and future [in French]. Ann Phys Fr 1985;10(6):645–657.
31. Salerno M, Brookeman JR, de Lange EE, Knight-Scott J, Mugler JP Jr. Demonstration of an alveolar-size gradient in the healthy human lung: a study of the reproducibility of hyperpolarized 3He diffusion MRI [abstr]. In: Proceedings of the Eighth Meeting of the International Society for Magnetic Resonance in Medicine. Berkeley, Calif: International Society for Magnetic Resonance in Medicine, 2000; 2195.
32. Fichele S, Woodhouse N, Swift AJ, et al. MRI of helium-3 gas in healthy lungs: posture related variations of alveolar size. J Magn Reson Imaging 2004;20(2):331–335.
33. Kirby M, Heydarian M, Svenningsen S, et al. Hyperpolarized 3He magnetic resonance functional imaging semiautomated segmentation. Acad Radiol 2012;19(2):141–152.
34. Tustison NJ, Altes TA, Song G, de Lange EE, Mugler JP 3rd, Gee JC. Feature analysis of hyperpolarized helium-3 pulmonary MRI: a study of asthmatics versus nonasthmatics. Magn Reson Med 2010;63(6):1448–1455.
35. Kauczor HU, Markstaller K, Puderbach M, et al. Volumetry of ventilated airspaces by 3He MRI: preliminary results. Invest Radiol 2001;36(2):110–114.
36. Lee EY, Sun Y, Zurakowski D, Hatabu H, Khatwa U, Albert MS. Hyperpolarized 3He MR imaging of the lung: normal range of ventilation defects and PFT correlation in young adults. J Thorac Imaging 2009;24(2):110–114.
37. Svenningsen S, Kirby M, Starr D, et al. What are ventilation defects in asthma? Thorax 2014;69(1):63–71.
38. Park T, Lee YJ. Covariance models for nested repeated measures data: analysis of ovarian steroid secretion data. Stat Med 2002;21(1):143–164.
39. Virgincar RS, Cleveland ZI, Sivaram Kaushik S, et al. Quantitative analysis of hyperpolarized (129) Xe ventilation imaging in healthy volunteers and subjects with chronic obstructive pulmonary disease. NMR Biomed http://www.ncbi.nim.nih.gov/pmc/articles/PMC3624045/. Published Oct 13, 2012. Accessed April 2014.
40. Cadman RV, Lemanske RF Jr, Evans MD, et al. Pulmonary 3He magnetic resonance imaging of childhood asthma. J Allergy Clin Immunol 2013;131(2):369–376, e1–e5.
41. Parraga G, Mathew L, Etemad-Rezai R, McCormack DG, Santyr GE. Hyperpolarized 3He magnetic resonance imaging of ventilation defects in healthy elderly volunteers: initial findings at 3.0 Tesla. Acad Radiol 2008;15(6):776–785.
42. de Lange EE, Altes TA, Patrie JT, et al. Changes in regional airflow obstruction over time in the lungs of patients with asthma: evaluation with 3He MR imaging. Radiology 2009;250(2):567–575.
43. Tschirren J, McLennan G, Palágyi K, Hoffman EA, Sonka M. Matching and anatomical labeling of human airway tree. IEEE Trans Med Imaging 2005;24(12):1540–1547.